# Chapter 3

## 3.1    Introduction

GO nanosheets have emerged as one of the excellent two-dimensional nanomaterials with a large surface area and are scattered with polar oxygenated groups containing $sp^2$ conjugated domains. The large surface area and nano-scale thickness of GO bestow the polymer with noteworthy enhancements in its properties [266,267]. The exceptional structure and excellent functional properties of GO enable charge transfer interactions with different organic conjugated polymer molecules [268,269]. Therefore, GO has gained great attention in the synthesis of GO/polymer hybrid nanocomposite materials and their numerous applications in the fields of electronics, optoelectronics, batteries, supercapacitors, etc. It is important to note that the work function of GO falls within the band gap of the polymer, which causes the complex charge transfer (CT) interaction. This interaction provides a way to explore the uses of GO/polymer composites for the enhancement of electronic as well as optoelectronic devices and to investigate the doping effect on either GO or the conjugated polymers by the counterpart. For example, Stylianakis et al. used modified GO with P3HT polymer and enhanced the device performance by 2 orders [270,271]. Further, Wang et al. demonstrated that the GO/Polymer nanocomposites have wide bands of electronic absorption due to $\pi$–$\pi$ interactions [272]. Gao et al. enhanced the conductivity of the polymer film up to 3.70 S m$^{-1}$ after doping with GO. The interactions between GO and P3HT endowed the composite with excellent properties, which neither of them possesses individually [273]. Liscio et al. used Kelvin probe force microscopy (KPFM) to probe the surface potential at a nanometric scale and found no significant charge injection barriers between the graphene sheets and the polymer [274]. Despite these reports, some crucial issues such as the very low solubility of graphene in common organic solvents like chloroform, the tendency to form aggregates and the weak charge transfer interactions between the polymer and nanostructure, random distribution of nanosheets in the polymer matrix, the formation of small area, low crystalline polymer thin film or need of post higher temperature thermal treatment, disorientation and disorder at the molecular level of the polymer and nanoparticle domains remain to be, resolved. Currently, intense research in the development of organic polymer-based semiconducting materials like polyaniline, polythiophene or their derivatives is ongoing [275,276]. Among these, the solution-

processable derivative of the polythiophene conducting polymer namely poly[2,5-bis(3-tetradecylthiophen-2-yl)thieno[3,2-b]thiophene] (PBTTT) has attracted immense scientific interest due to its superior charge transfer characteristics and the ability to self-organize into ordered structures [277,278]. The self-organizing property of PBTTT is of particular interest because of the one-dimensional electronic property of the $\pi$-conjugated polymer chains, which can modify the interchain stacking resulting from the $\pi$–$\pi$ interactions. The alkyl side chains of PBTTT provide additional ordering through inter-molecular interdigitation and enable solubility in common organic solvents. Crystallization induced by the $\pi$–$\pi$ stacking, alkyl side chain interactions, and changes in solubility allow increased crystallization length and efficient charge transfer in PBTTT films [279-281]. Therefore, to garner the exceptional electronic properties of graphene nanosheets and the good processability as well as modulable electronic characteristics of PBTTT, we fabricated composite thin films comprising these two materials. In recent years, $\pi$-conjugated organic semiconductors with nanofillers have opened up new opportunities and provided a path to modify their self-assembly and electronic properties to suit particular applications. Therefore, a variety of processing methods have been reported for the dispersal of both graphene nanoparticles and GO-derived fillers into the polymer matrices and thin films. There are several problems related to the reported techniques such as the modification of GO sheets as mentioned earlier, the limitation of the device performance due to the use of surfactant, the complexity of the thin film fabrication process, the high-temperature annealing step limiting the film conductivity and further applications in flexible substrate-based electronics and optoelectronics devices [282]. Therefore, we have introduced a new methodology for synthesis and film processing that resolves these challenges by enhancing the processability of the polymer nanocomposite solution, thereby augmenting the alignment and molecular-level assembly of the polymer and nanoparticle domains. It consists of three steps: (i) phase transfer of GO from water to chloroform using ultrasonication (without any surfactants)(ii) formation of the polymer nanocomposite in chloroform via ultrasonication and (iii) use of the facile FTM technique for fast growth in synthesizing the polymer nanocomposite thin film at the air-liquid interface [283,284]. In this study, we have synthesised GO nanosheets by an improvised Hummer's method. Before the formation of the PBTTT/GO composite, GO was transferred from water to chloroform via ultrasonication without surfactant. Chloroform-dispersed GO was used for the preparation of the PBTTT/GO

solution. Further, to obtain fast growth, large area, and self-assembly of composite polymer nanocomposite thin film, liquids with high surface energy namely ethylene glycol and glycerol were employed in a 1: 1 ratio. The as-deposited film was characterized for its morphological, structural, spectral, and electrochemical properties and compared with a pristine polymer film. Finally, the polymer nanocomposite film was used in the fabrication of a thin film transistor, which demonstrated an improved device performance with a better on/off ratio in ambient conditions.

## 3.2 Results and Discussion

### 3.2.1 Characterization of GO nano-sheets

The surface morphology of the GO nanosheets was characterized using SEM and TEM as shown in Fig. 3.1(a and b). The size of GO sheets ranged from a few tens of nanometers to a few micrometres. The SEM image shows randomly oriented and crumpled thin sheets having wrinkles and folds. However, TEM portrays transparent bends and wrinkles on the GO nanosheets at several places as can be seen in Fig. 3.1(b). These might have developed during the oxidation process due to the formation of defects and the introduction of functional groups carrying $sp^3$ hybridized carbon atoms. The GIXD pattern of graphene oxide indicates an intense peak around 10.51°, which corresponds to the (001) diffraction peak of graphene oxide (Fig. 3.1(c)). The interlayer spacing of graphene oxide was calculated to be 0.84 nm. To calculate the number of layers, we used. the relation $Lc = 0.9\lambda/FWHM.\cos\theta$ (Scherrer's formula), where Lc is the coherence length and $\lambda$ is the wavelength of the X-ray. Although Scherrer's formula is conventionally employed to determine the crystallite size, an exact calculation is not possible due to the presence of disorder in the polymer crystallites. This is why it is termed coherence length Lc and is used in the estimation of the number of GO layers. The $L_c$ for GO was found to be ~ 6.1 nm, which is equivalent to ~7 layers when divided by the interlayer spacing of GO (0.84 nm). The thickness of GO nanosheets was also measured using AFM and found to be 6.10 nm, which validates our XRD result. The SAED analysis (inset of Fig. 3.1(c)) again authenticates the structure exemplified by the GIXD pattern. Notably, a similar GIXD pattern was obtained after the phase transfer of GO, which has been shown in a later section. Fig. 3.1(d) shows the UV-visible absorption spectrum of GO nanosheets with the main absorption peak appearing at 229 nm and a shoulder at 300 nm. The main absorption peak is attributed to the $\pi$–$\pi^*$ transitions corresponding to the

aromatic C=C bond. The shoulder peak is attributed to the C=O bonds. Moreover, the FTIR spectrum (inset of Fig. 3.1(d)) illustrates the different types of oxygen functionalities and C=C at 1615cm$^{-1}$. The wide peak at 3396 cm$^{-1}$ is ascribed to the O–H stretching vibrations from COOH, C–OH and $H_2O$. The broadening of the O–H band may be due to the presence of intercalated $H_2O$ molecules between the graphene oxide sheets. The strong band at 1734 cm$^{-1}$ is attributed to the stretching vibrations of the C=O bonds in carboxylic acid and carbonyl groups. The bands at 1223 cm$^{-1}$ and 1054 cm$^{-1}$ are usually attributed to the C–OH stretching vibrations and C–O(epoxy) groups, respectively. The C=C skeletal vibrations from non-oxidized graphitic domains result in the peak at 1623 cm$^{-1}$, which could also be due to the stretching deformation vibrations of the intercalated water. Therefore, the results obtained using different techniques confirm the formation of GO nanosheets having a honeycomb structure with C=O, C–OH, and O–H functional groups at different sites (Fig. 3.1(e)). Further, the degree of oxidation calculated from the FT-IR spectrum was to be 81%. The detailed procedure for the calculation of the degree of oxidation has been given as [285] :

The following procedure was followed for quantitative analysis of the FTIR spectrum:

1. The resulting spectrum was multiplied by -1 so that all peaks are reversed.

2. The baseline is subtracted from raw data using origin18 software (baseline mode-create baseline –baseline treatment) then different peaks were found and fitted peaks.

3. Different peaks area were calculated viz. peak 1 to peak 12. Peak 1 corresponds to C=C bond stretching at 1615.38 cm$^{-1}$ having fitted area 566.06.

4. The sum of all oxygen-related bands is calculated by subtracting the aromatic C=C band at 1615.38 cm$^{-1}$ from the total spectra i.e. aromatic C=C band area is subtracted from the total area(by adding areas covered by all peaks).

5. Ratio of oxygen-related band area to the total area is calculated as follows.

$$\frac{A(ORB)}{A(TOTAL)} = \frac{A(TOTAL) - A(C = C)}{A(TOTAL)} = ORB:TOTAL$$

The above equation is used as a measure of the degree of functionalization of the graphite sheet. Using the above equation ORB: TOTAL ratio came out to be 0.81. The fitted FTIR curve of GO is shown in Fig.3.2.The Raman spectrum of GO measured using a 532 nm laser as the excitation source shows D and G bands at 1364 cm$^{-1}$ and 1590 cm$^{-1}$, respectively (Fig. 3.1(f)). While the G band is the first-order Raman band for all the sp$^2$ hybridized carbon materials, the D band may arise from certain defects such as vacancies, grain boundaries, and amorphous carbon species. The intensity ratio of these two bands specifies the quality of the product. The integral intensity ratio of these two peaks scales with the degree of graphitic ordering in the carbons. The ratio of the peak intensities i.e. $I_D/I_G$ was found to be 0.89; the intensities were calculated by curve fitting of the Raman spectrum as shown in Fig. 3.3.
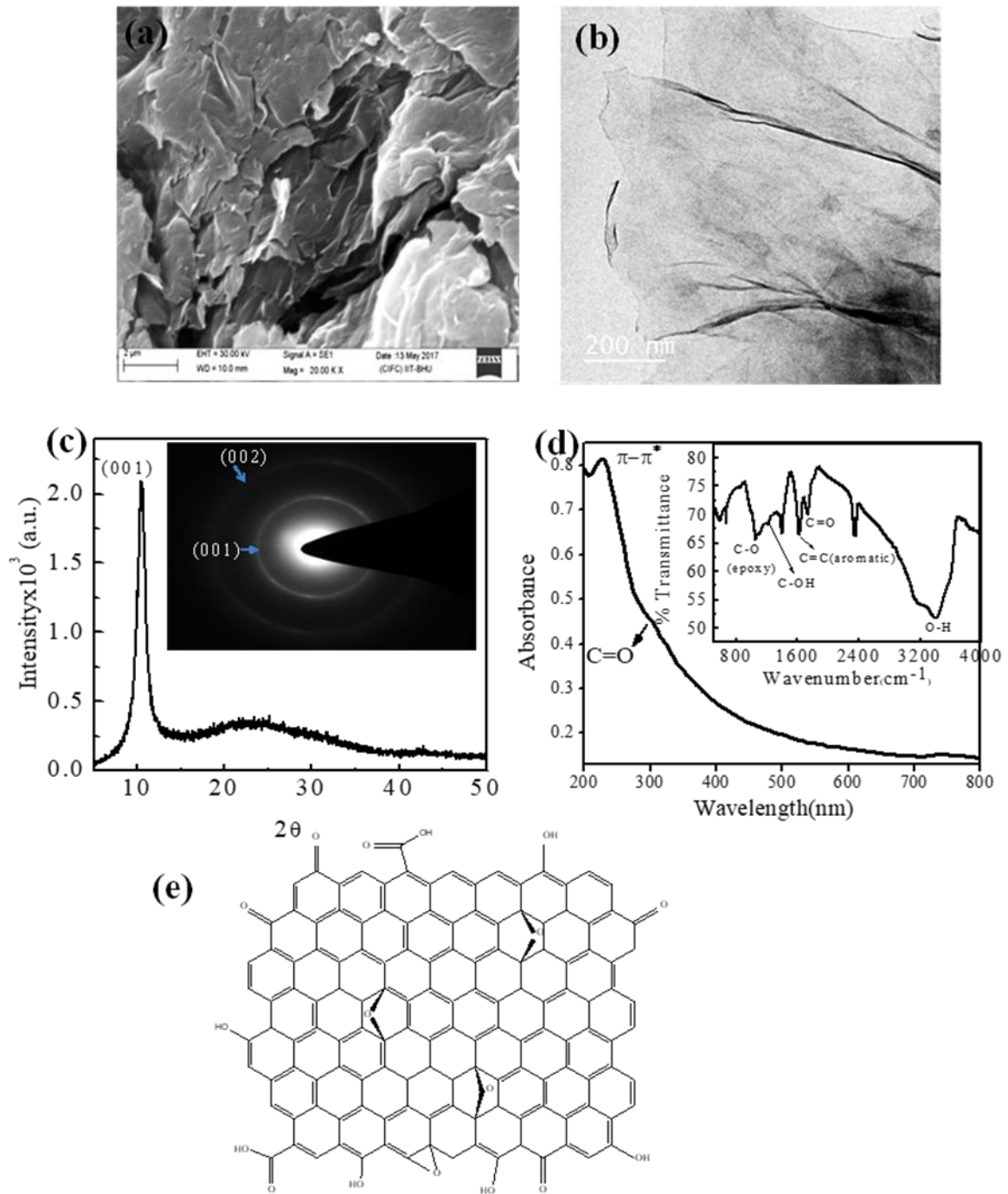
**Fig. 3.1 (a) SEM and (b) TEM images of the as-synthesized GO. (c) XRD pattern of the GO powder. Inset shows the SAED pattern of the as-synthesised GO powder. (d) UV-vis spectrum (inset shows the FT-IR spectrum), and(e) Schematic structure of the GO sheet. (f) Raman spectrum of GO when excited using a 532 nm laser source.**
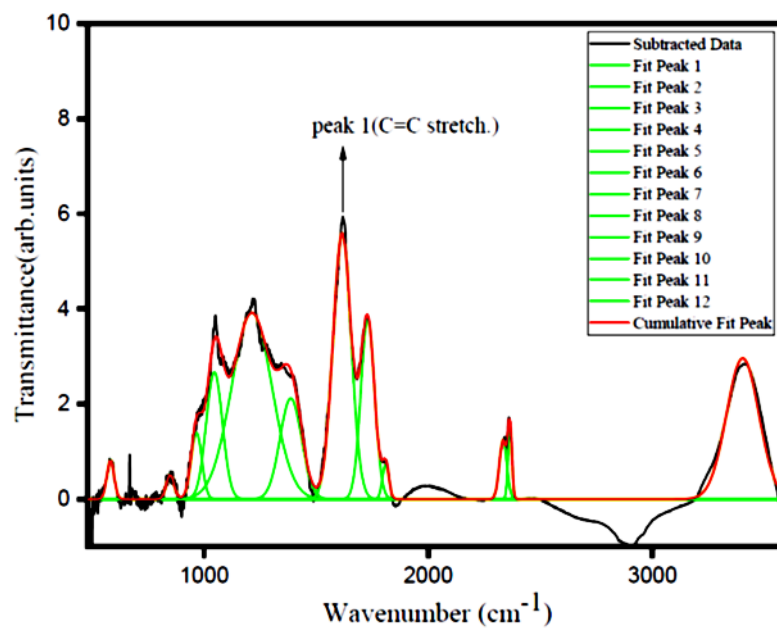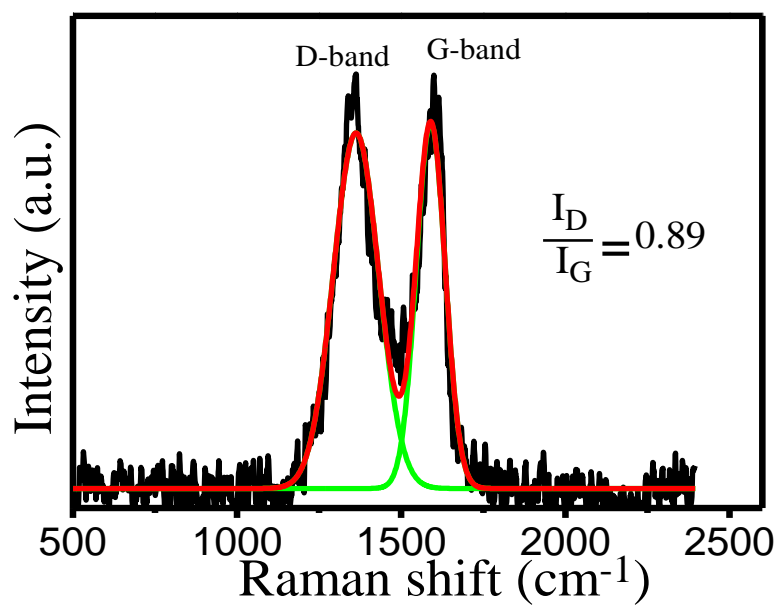
**Fig.3.2 Fitted curve of FT-IR spectrum of GO.**



**Fig.3.3 Fitted curve of Raman spectrum of GO.**

**3.2.2 Characterization of the nanocomposite film**

**3.2.2.1. Morphological study**

The SEM image of the PBTTT/ GO nanocomposite FTM film presents a clear picture of the GO nanosheets in the polymer film matrix (Fig. 3.4(a)). However, no signature GO nanosheets are observed in the pristine PBTTT FTM film (Fig. 3.4(b)). Fig. 3.4(c) shows the TEM image of PBTTT/GO nanocomposite film over a Cu grid, while, the inset shows the PBTTT/GO hybrid film at higher magnification. Intensive investigation of the composite FTM film via TEM shows uniform distribution of GO in the PBTTT polymer matrix and has also been validated by fluorescence imaging (Fig. 3.4(e)). Further, the SEM and TEM data were put together to reveal the decoration of the PBTTT polymer nanostructure over the GO sheets. HR-TEM (Fig. 3.4(d)) of the same demonstrates that only the (010) plane corresponds to $\pi$–$\pi$ stacking. Similar highly-oriented and crystalline films with edge-on lamellar morphology of polymer have been reported earlier by Brinkmann et al.[286]. The spacing between the lattice fringes was measured to be 0.39 nm, which is equivalent to the d-spacing of the (010) plane or $\pi$–$\pi$ stacking distance of the PBTTT backbones. This confirms the presence of a $\pi$–$\pi$ stacked lamellar structure of the polymer backbones with an edge-on arrangement over the substrate in the hybrid film. This is highly desirable for high-mobility planar devices like transistors because of the anisotropic nature of the polymer. Further, the SAED pattern of the PBTTT/GO nanocomposite films(inset of Fig. 3.4(d)) validates the amorphous nature of polymer nanocomposite.
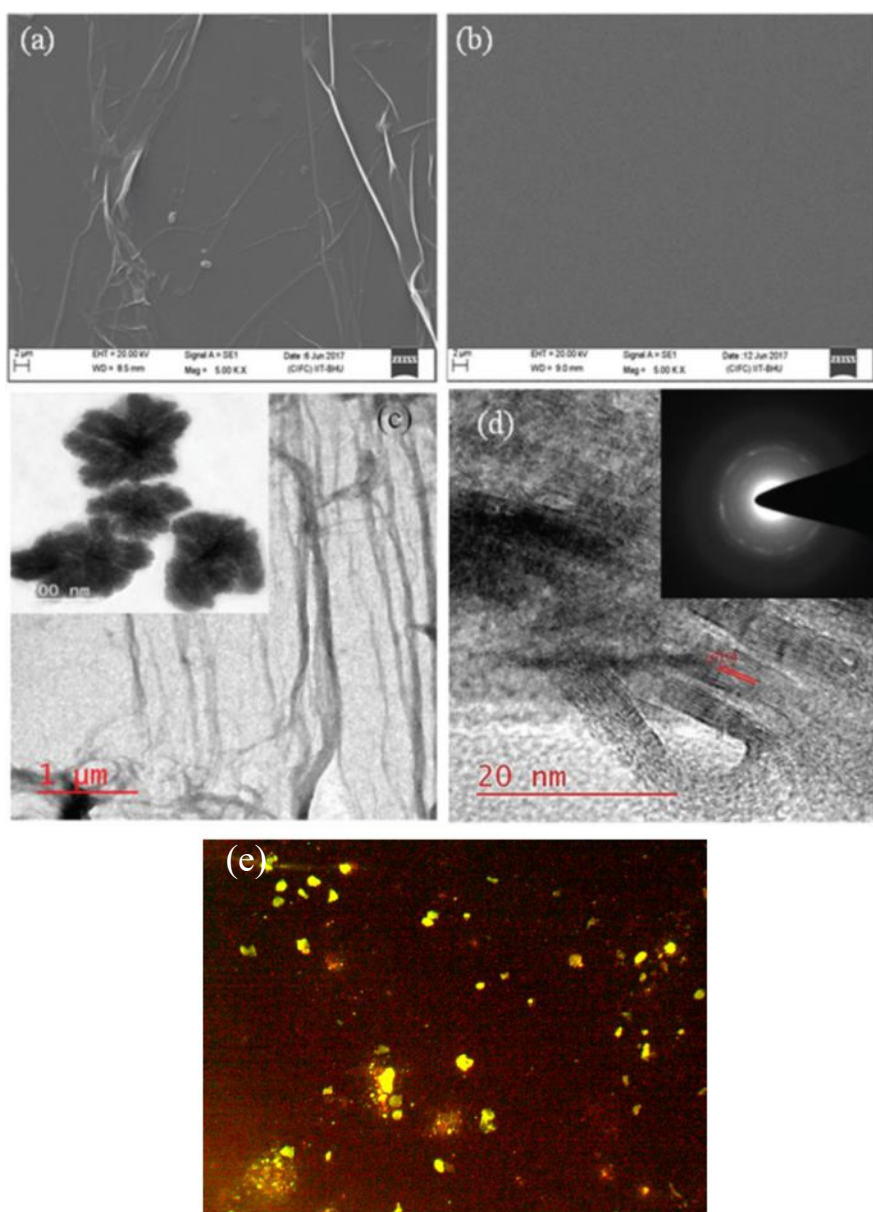
**Fig. 3.4 SEM image of (a) PBTTT/GO composite and, (b) pristine PBTTT FTM film over a solid substrate. (c) TEM image of PBTTT/GO composite FTM film over Cu grid. Inset shows the PBTTT/GO composite FTM film at a higher magnification. (d) HR-TEM image of the composite film showing the (010) plane. Inset shows the SAED image of the PBTTT/GO composite FTM film. (e) Fluorescence image (100 x) of PBTTT/GO film formed by FTM technique.**

Fig. 3.5(a–f) shows the AFM topography, phase image and KPFM images (scan area 3.5 mm x3.5 mm) of PBTTT/GO nanocomposite FTM film and pristine PBTTT thin film, respectively. AFM topography of the two films demonstrates apparent morphological differences (Fig. 3.7(a and d)) with a bigger domain size for PBTTT/GO nanocomposite having an average area roughness of 2.68 nm. This confirms the formation of a very smooth film with nano-level roughness. The bigger domain size and similar height profile of PBTTT/GO film as compared to pristine polymer demonstrates the connected morphology via GO (Fig. 3.5(a and d)), which enhances the connectivity among domains. TEM and SEM images show GO sheets, over which the polymer nanocrystallites are lying. Due to the absence of GO sheets in the pure polymer matrix, smaller domains are formed and remain either isolated or connected via amorphous long polymer chains that limit conductivity and mobility. The properties of the films were also investigated via phase imaging, which again confirmed the visible phase difference between the two films with the difference in phase angle. There are clear differences in the phase image showing GO sheets decorated with polymer similar to AFM topography (Fig. 3.5(b and e)). It is important to note that AFM topography, phase imaging and KPFM imaging were carried out simultaneously. Therefore, KPFM was carried out in the same region as shown in Fig. 3.5(a and d) to measure the surface potential contrast (SPC) of the film surface. It is quite obvious from Fig. 3.5(c and f) that SPC images of the films are not similar. The SPC height of the composite film obtained via KPFM reveals a uniform surface potential with 16 meV potential height, which indicates the absence of a height barrier between the nanosheets and polymer aggregates. A similar absence of potential barrier between the polymer and nanosheets has been reported previously[274]. Their variation in the SPC height and average between the two films arises only due to larger domains and the presence of nanosheets. This discloses the differences in the electronic property and surface energy/potential of the films, which were confirmed further by CV measurement (shown later).
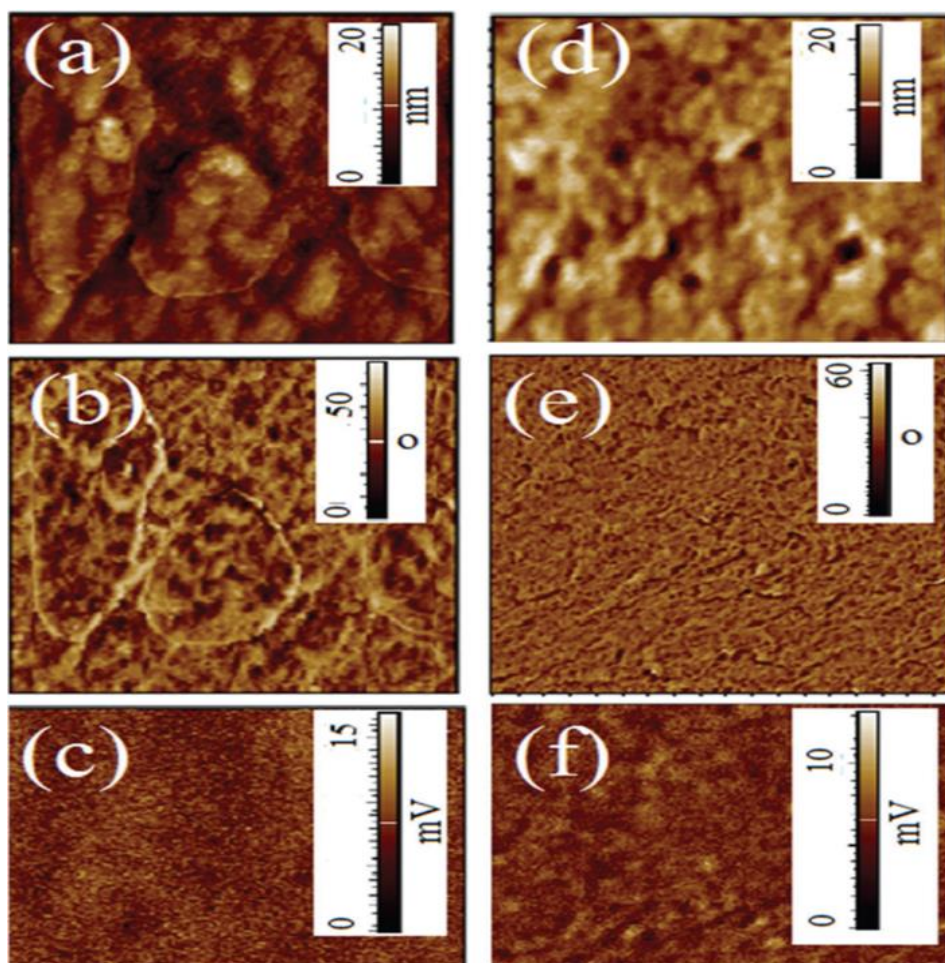
**Fig.3.5 AFM topography, phase image and KPFM image (scan area – 3.5 mmx3.5 mm) of (a–c) the PBTTT/GO nanocomposite and (d–f) the pristine PBTTT FTM film, respectively.**

### 3.2.2.2. Structural analysis

GIXD patterns(equipped with an in-plane diffractometer and out-of-plane moving detector) of GO, pristine and hybrid films prepared by FTM with a grazing angle of 0.21 are shown in Fig. 3.6(a–c). The GIXD pattern of graphene oxide indicates an intense peak around 10.51 corresponding to the (001) diffraction peak of GO, which is the same as the synthesized GO. The interlayer spacing of graphene oxide was calculated to be 0.84 nm according to the diffraction peak at $2\theta = 10.51°$ using Cu-K$\alpha$ radiation ($\lambda = 1.54056$ Å). Further, the FTM film of PBTTT/GO nanocomposite shows only one set of reflections such that the three low-angle diffraction peaks are indexed at (100), (200), and (300). A shift of the (100) peak by 0.11° towards a lower angle was observed for the composite

film compared to pure PBTTT. This shift might have arisen due to the CT interaction between polymer and filler. Notably, the GO peak was absent in the GIXD of the composite film. However, intense morphological characterization reveals the presence of GO in the polymer matrix. This confirms the presence of a percentage very low GO fraction in nanosheets (<3%), in which the plane diffractometer and out-of-plane moving detector) of GO, are out of the detection limit. Analysis of GIXD peak intensities of pure PBTTT reveals a similar set of reflections as the PBTTT/ GO composite film but with lower intensity. This demonstrates the substantial growth of domains in the nanocomposite films developed via FTM without thermal preparation as shown in TEM and AFM images. It is important to note that HR-TEM shows the (010) plane, while GIXD shows only the (100) plane, which confirms the highly edge-on orientation of the polymer film. Edge-on orientation is highly desirable for planar devices such as OTFTs because of the anisotropic nature of mobility (maximum along the direction of either the polymer chain or π–π stacking).
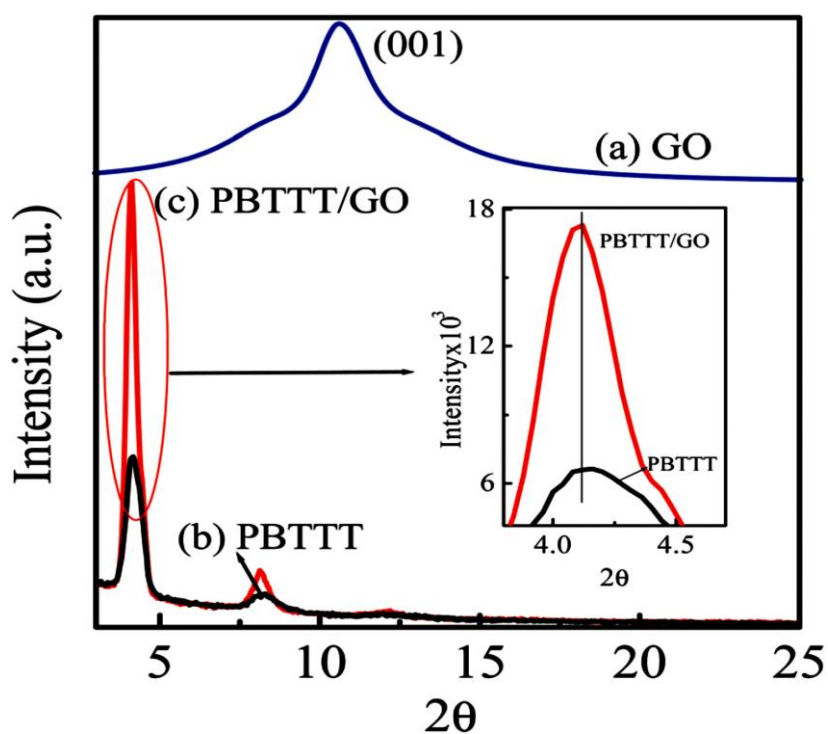


**Fig.3.6 GIXD of (a) GO cast from chloroform, (b) PBTTT/GO hybrid, and (b) PBTTT FTM film with grazing angle 0.21°.**

### 3.2.2.3. Spectral analysis

To examine the interactions between PBTTT and GO, FTIR and UV-vis absorption were investigated and compared with the pristine one as shown in Fig. 3.7(a and b). The peak at 756 cm$^{-1}$ in the FTIR spectrum of pristine PBTTT corresponds to the C–S stretching vibration in the ring, which shifted to a lower wavenumber i.e. 750 cm$^{-1}$ in the PBTTT/GO composite. A new peak at 1076 cm$^{-1}$ for the PBTTT/GO composite corresponds to C–O vibrations from the epoxy groups in GO. The peak around 875 cm$^{-1}$ in both pristine PBTTT and PBTTT/GO composite corresponds to the C–H out-of-plane deformation (ring). The symmetric C=C stretching vibration bands of the thiophene rings are found around 1464 cm$^{-1}$. On the other hand, the antisymmetric CQC stretching vibration bands of the rings appeared around 1517 cm$^{-1}$. Fig. 3.7(b) displays the normalized electronic absorption of PBTTT/GO nanocomposite and pristine PBTTT films prepared by the FTM technique. Strong absorption peaks appear at 549 nm and 543 nm with right shoulder peaks at 579 nm and 574 nm, respectively. The broadening and red shifting of the PBTTT/GO hybrid peak compared to the pristine PBTTT films demonstrates charge transfer (CT) interactions between the polymer and GO. It is known that the absorbance spectrum would shift either towards blue or red with changes in the ratio of vibronic peak intensities ($A_{0–0}/A_{0–1}$) caused by molecular interactions [287]. Therefore, it can be observed from UV-vis absorption spectra of the composite film that the peak is red-shifted compared to that of pristine PBTTT film which confirms the existence of interaction between polymer and GO nanosheets. It is also known that the degree of intrachain ordering can be further manifested in the absorbance spectra of thin films of thiophene [288,289]. The improvement in conjugation length and degree of intrachain order in the composite film has caused an increase in the ratio between the lowest energy peak and the next replica peak as seen in Fig.3.7(b). Therefore, the enhancement in peak ratio indicates the augmented intrachain order and extended conjugation lengths in the composite film. It has been found that GO can induce polymer chains to form nanostructures or nanowhiskers on GO or RGO surfaces [290-292]. Herein, we infer that the increase of peak ratio ($A_{0–0}/A_{0–1}$) in PBTTT/GO composites originated from the increased conjugation lengths in the presence of nano-sheet since the same FTM has been used for casting both the samples.
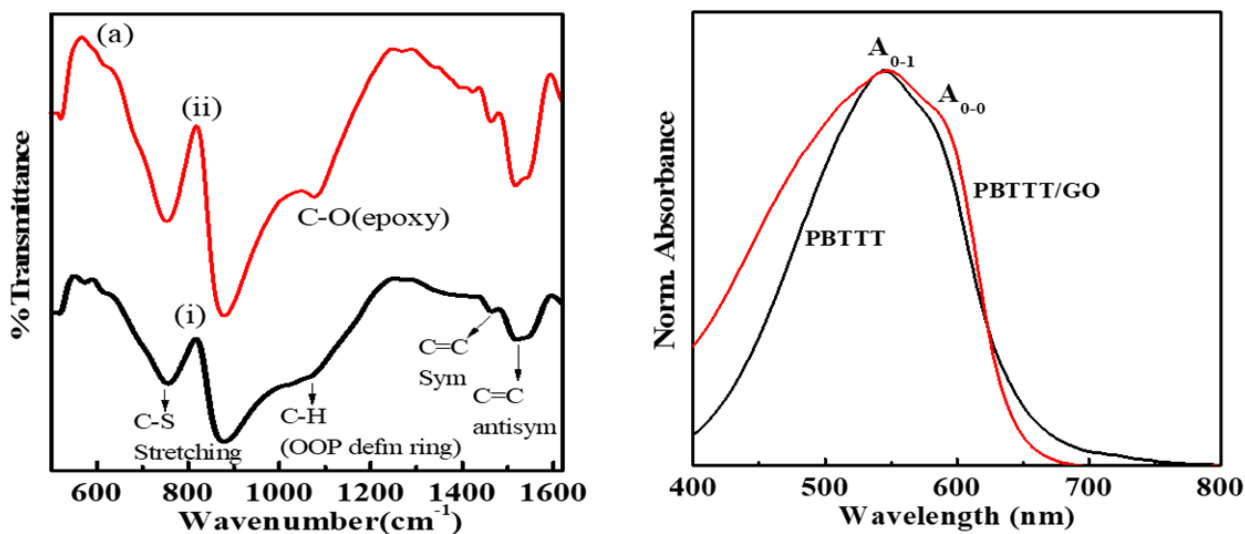
**Fig.3.7 (a) FTIR spectra of (i) PBTTT and (ii) PBTTT/GO, (b) Normalized absorption spectra of PBTTT and PBTTT/GO nanocomposite FTM films over ITO coated glass substrate**.

### 3.2.2.4. CV and estimation of HOMO and LUMO

CV measurement was employed to examine the oxidation potential and estimate the HOMO levels in both films as shown in Fig.3.8. The HOMO level was estimated using equation $E_{HOMO} = -e(4.4 + E_{ox}(onset))V$ and was found to be 4.96 eV and 5.01 eV for the composite and pristine polymer films, respectively. A similar observation has been reported by Istif et al., where the presence of GO induced the formation of polymer nanostructure and the existence of charge transfer interaction caused a reduction in HOMO energy level [137]. Thus, the shifting of the HOMO level, as well as the nature of absorption spectra, showcases changes in the electronic property of the composite material. It is well-known that different morphologies demonstrate different energy levels and work function of electrons, which are directly related to the morphology and electronic coupling between the polymer chains, respectively [293,294]. CV is also connected to the work function of materials because it monitors the ejection of electrons from the energy level of molecules (HOMO) to the surface exterior. Hybridization of PBTTT with GO causes a shift of the oxidation peak, which is completely different from that of the pure polymer.

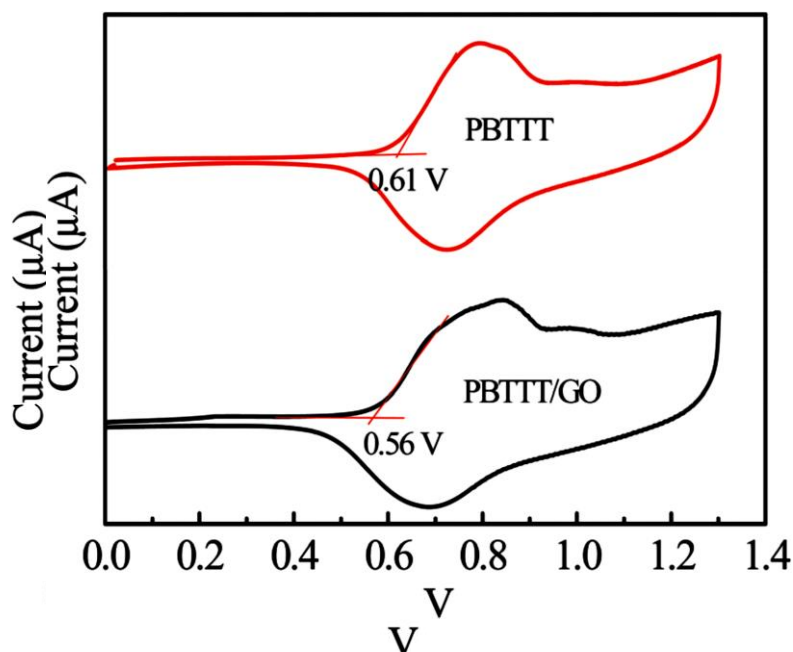$$E_{HOMO} = -e(4.4 + E_{ox}(onset))V \qquad (3.1)$$

**Fig.3.8 Cyclic voltammetry of the PBTTT/GO nanocomposite and pure FTM films over ITO-coated glass substrate.**

### 3.2.2.5. Electrical characterization

To probe the mobility and the electronic parameters of the as-prepared films, OTFTs were fabricated by depositing Au electrodes on the top. It is noteworthy that the synthesis, film deposition, fabrication of the device and measurements were performed at room temperature with 54% RH in the dark. The I–V plots of the pristine polymer film have been given in Fig.3.9(a,b) for comparison. The representative results of I–V for the composite thin film have been given in Fig.3.10(a and b). Preliminary investigation reveals the well-known p-type $I_d$–$V_d$ output and $I_d$–$V_g$ transfer characteristics. The performance of TFTs is highly dependent on the homogeneous dispersion of nanomaterials in the polymer matrix. Therefore, we transferred the film to 10 different places and measured the $I_d$–$V_g$ for each, which were all almost identical curves with small variations in the current as shown in Fig. 3.11. The parameters of field effect mobility (μ) and on/off ratio were calculated in the saturated regime using Eqn (3.2).

$$I_D = \frac{W}{L} \ \mu C_i (V_g - V_{th})^2 \qquad\qquad (3.2)$$

where $I_d$ is the drain current, W is the channel width and L is the channel length, $C_i$ is the capacitance per unit area, and Vg is the applied gate voltage, $V_{th}$ is the threshold voltage.

Using the above equation, μ of the composite film was found to be~0.112 cm$^2$ V$^{-1}$ s$^{-1}$ at -30 V which is more than 4 times for pristine polymer and one order enhancement in on/off ratio ($10^3$) in ambient as compared to pristine polymer film (the transfer curve for the pristine polymer is shown in Fig. 3.11(b)). The low value of the on/off ratio in our case can be justified by considering the condition of measurement and the concentration of 2d nanosheets. We carried out all I–V measurements in an open ambient setting with 54% relative humidity, which could be the reason for the low on/off ratio [276]. The incorporation of 2d nanosheets reduces the on/off ratio as well [274]. However, the obtained value of mobility for the composite film is high for anisotropic film compared to those reported earlier [274,281]. Thus, the obtained value of high mobility can be attributed to the surface morphology, where lamella of PBTTT are synergistically supported by GO nanosheets as shown by the microscopy images, GIXD, CV, and the scheme in Fig. 3.12(c). Surface morphology confirms the decoration of GO sheets with the larger domains of PBTTT polymer. Meanwhile, the HR-TEM image and GIXD reveal the self-assembly of a highly edge-on oriented nanocomposite film, which is highly desirable for planar devices. Thus, the synergistically supported lamella of PBTTT and GO together enhance the crystallinity and facilitate charge transport as well. These, in turn, enhance the output current and mobility of the composite [268]. Further, the broadening and red shift of the absorption peak validate the presence of CT interactions between the polymer and GO sheets with extended conjugation length and planarity of molecules. Moreover, doping of GO and polymer on each other to a certain extent according to their respective compositions in the GO/polymer hybrid complex is a well-documented phenomenon [272]. Remarkably, several types of conduction pathways are possible in composite materials such as conduction along the crystalline polymer chains, conduction across the amorphous polymer chains, conduction between the polymer chains and the nano-fillers, and conduction between the conducting fillers via polymer chains, which indicates the existence of percolative character. This percolation path facilitates the conduction mechanism by reducing the path resistance between the source and drain electrodes. CV reveals the change in oxidation potential, which confirms the tuning of electronic properties and positions of the HOMO and LUMO levels. Tuning of the HOMO level may further facilitate the injection efficiency of charge carriers across the electrodes and active materials, thereby enhancing the mobility of materials [296].
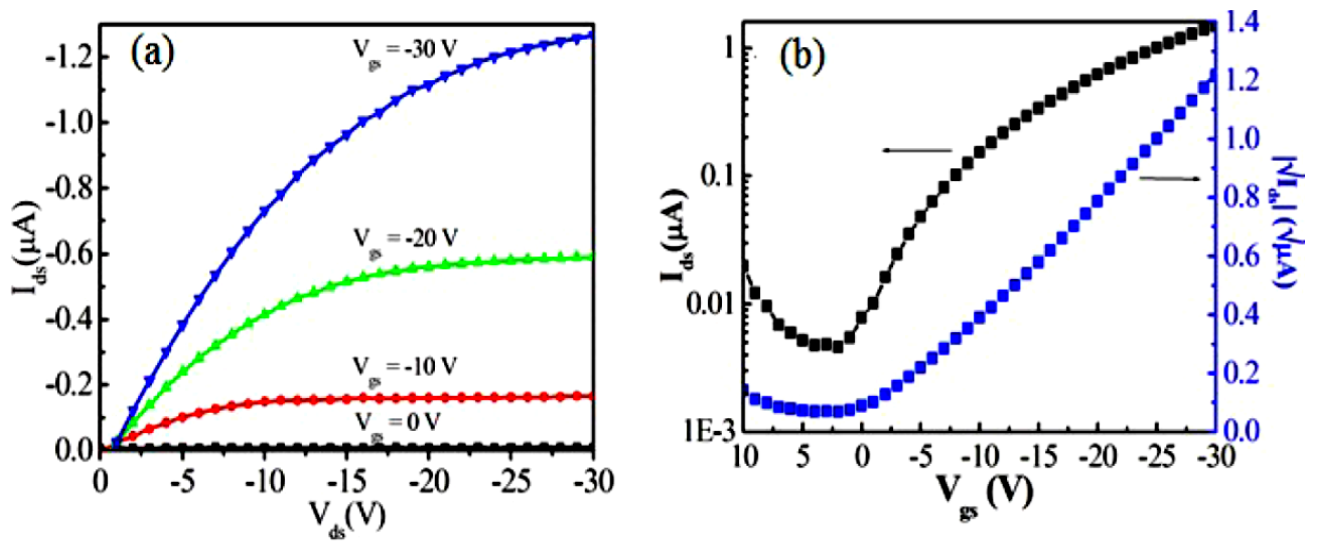
**Fig.3.9 (a) $I_{ds}$-$V_{ds}$ output and (b) transfer characteristics of pristine PBTTT thin film.**
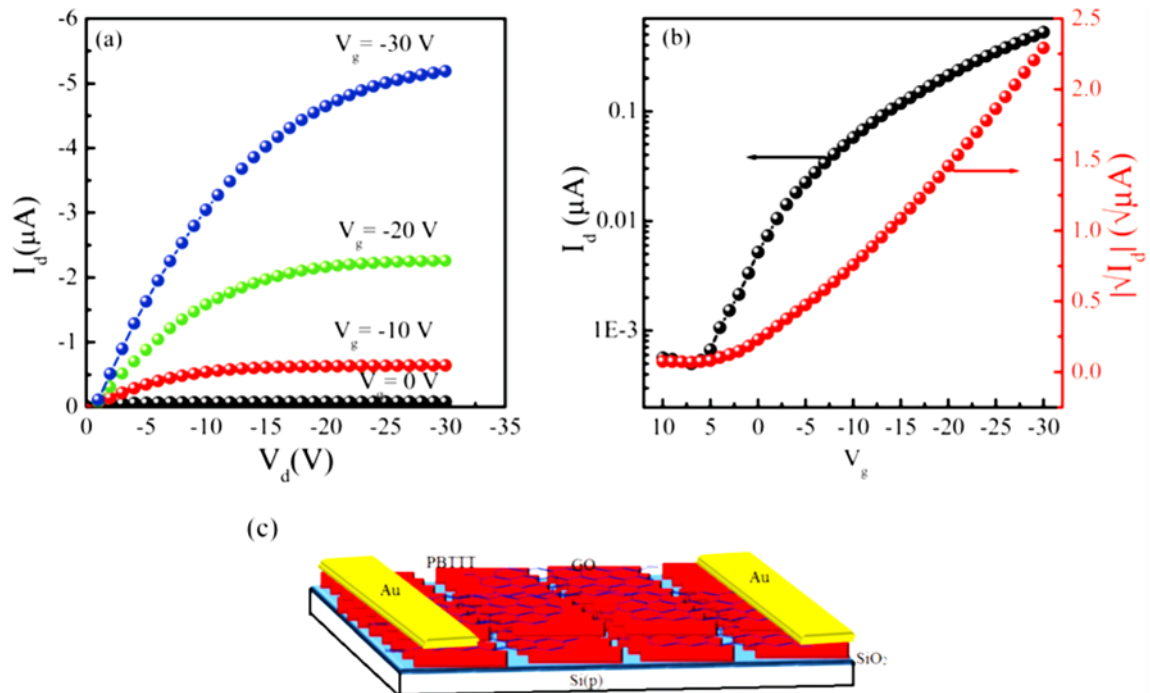
**Fig.3.10** (a) $I_{ds}$–$V_{ds}$ output and (b) transfer characteristics of PBTTT/GO nanocomposite thin film. (c) Schematic of the thin film transistor containing the composite thin film with uniform distribution of GO sheets in a crystalline polymer matrix.
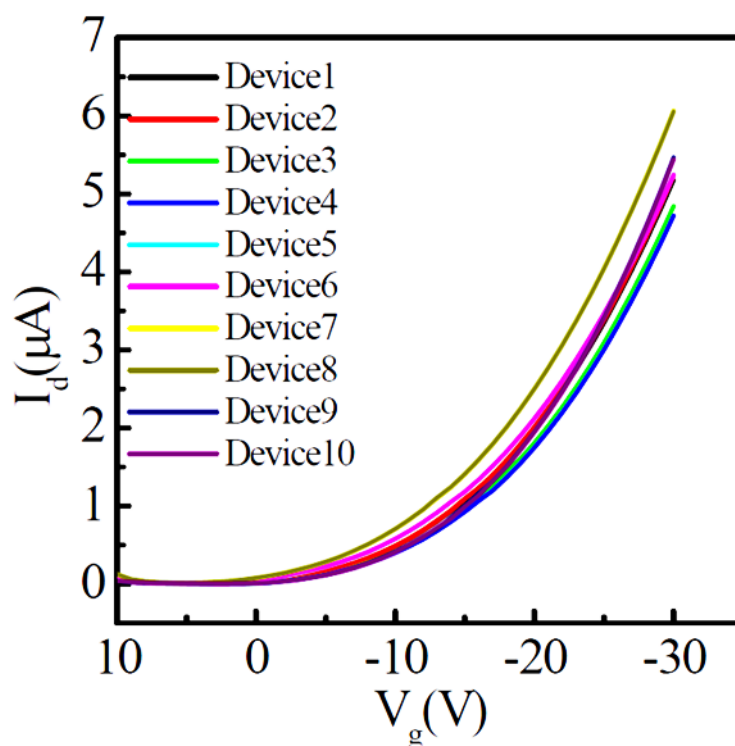
**Fig.3.11 $I_d$-$V_g$ transfer characteristics of PBTTT/GO nanocomposite thin film at 10 different places at $V_d$= -30 V.**

## 3.3. Conclusions

We have presented a facile and fast thin film fabrication technique 'FTM' for the formation of self-assembled highly edge-on oriented PBTTT/GO composite thin film with a large area at the air-liquid interface. Morphological, spectral, and structural characterizations validated the successful synthesis of GO. Multiple morphological characterization techniques viz. SEM, TEM, AFM, SAED etc. confirmed the formation of homogeneously dispersed nanosheets in the polymer matrix with interconnected crystalline domains. GIXD and HR-TEM confirmed the formation of highly edge-on oriented crystalline nanocomposite film. Spectral characterization revealed the presence of interactions between the polymer and nanosheets. Further, CV revealed the change HOMO level as well as electronic properties upon formation of the composite film. Finally, electrical investigation of the film configures in OTFTs revealed high mobility (0.112 cm$^2$ V$^{-1}$ s$^{-1}$) and an on/off ratio (10$^3$)in ambient conditions. Therefore, we have

shown a successful method for fast self-assembly of composite thin films using the FTM technique for better device performance and parameters such as high mobility.